Robotica: (2021) volume 39, pp. 772–786. © The Author(s), 2020. Published by Cambridge University Press.
doi:10.1017/S0263574720000715

Importing the Human Factor into Safe Human–Robot Interaction Function Using the Bond Graph Method

Po-Jen Cheng†, Hsiang-Yuan Ting‡ and Han-Pang Huang‡*

†*Department of Product Development, TECHMAN ROBOT Inc., Taoyuan, 33383, Taiwan, R.O.C.*
‡*Department of Mechanical Engineering, National Taiwan University, Taipei, 10617, Taiwan, R.O.C.*

(Accepted July 3, 2020. First published online: August 12, 2020)

SUMMARY
The variable stiffness actuator (VSA) is helpful to realize the post-collision safety strategies for safe human–robot interaction.[1] The stiffness of the robot will be reduced to protect the user from injury when the collision between the robot and human occurs. However, The VSA has a mechanism limit constraint that can cause harm to users even if the stiffness is minimized. Accordingly, in this article, a concept combining danger index and robust fault detection and isolation is presented and applied to active–passive variable stiffness elastic actuator (APVSEA). APVSEA can actively change joint stiffness with the change of danger index. Experimental results show that this concept can effectively confirm the fault mode and provide additional protection measures to ensure the safety of users when the joint stiffness has been adjusted to the minimum.

KEYWORDS: Safe; Human–robot interaction; Bond graph method; Fault detection; Variable stiffness actuator

1. Introduction

Human–robot interaction is one of the spotlight robot research topics.[2–4] The distance between the robot and human is getting closer and closer when people interact with robots. The idea is simple and can be directly applied to industrial robot arms. In order to ensure that the interaction between human and the robot will not cause damage to human or the robot, safety strategy issues should be considered in the design of the robot.[5,6] Safety strategies for human–robot interaction can be divided into two types, pre-collision and post-collision. The pre-collision safety strategy is to change the robot's motion speed or trajectory for keeping the distance between human and the robot before the collision.

Oppositely, the post-collision safety strategy ensures that when the collision occurs, the impact force does not exceed acceptable tolerances for various parts of the body or damage the robot. How to minimize the impact force during impact is one of the most important research topics of human–robot interaction.[7]

In order to absorb the impact force, the most common method is to coat the whole-body robot with the viscoelastic covering[8] or to adopt compliant joints.[9] Variable stiffness actuator (VSA) is one of the compliance mechanisms that its stiffness can be adjusted by controlling a spring between the motor and the output of the mechanism.[10–13] Wolf has designed an intrinsically compliant joint for robots.[14] However, all the mechanism of the robot or machine have limit constraints. Even if the

* Corresponding author. E-mail: hanpang@ntu.edu.tw

stiffness of the mechanism has been adjusted to a minimum, excessive speed of the robot may still put humans in a dangerous situation. Moreover, although flexible actuators allow robots to interact safely with humans, when they fail unexpectedly, they can still cause injuries to the user, an additional means to identify errors or unexpected situations is therefore necessary.

To solve the unexpected situation problems, Li et al.[15] proposed a new continuous adaptive impedance controller, which allows the robot to safely interact with the environment under the desired impedance model and stop immediately in case of unforeseen and unexpected safety problems, but it is not possible to identify other component failures using this method.

Through the fault detection and isolation (FDI) method, system errors can be identified and corresponding control methods can be selected. This is very important for the safety and management of the control system.[16–19] In order to choose an advisable modelling formalism for FDI, many studies use the Bond Graph tool because of its good structural and causal properties.[20–23] Besides, some other studies have used quantitative methods to generate the redundancy relationship (analytical redundancy relationships (ARRs)) to enhance the robustness of fault detection.[24–26] Additionally, in order to improve the accuracy for determining faults of the FDI method, Cheng's study based on the bond graph method proposed a robust fault detection and isolation (RFDI) method that can monitor the potential false alarms.[27]

The bond graph method is a model language modeled on multidisciplinary engineering systems. Therefore, a multidomain system, such as mechanical engineering, electrical systems, chemical and electromagnetic engineering, can be integrated using the same modeling approach. For example, Liu and Yu develop a fault diagnosis methodology based on the bond graph method to achieve FDI in electromechanical actuators.[28] Likewise, Mojallal and Lotfifard presented a method based on a hybrid bond graph theory to get the properties of doubly fed induction generator. Accordingly, the fault of these generators can be detected and isolated.[29]

How to sense the posture and position of human in space is also one of the key issues for the safety strategy of human–robot interaction. Kinect (Microsoft, Redmond, WA, USA) can easily be used to obtain depth and position information of various objects in space. Therefore, applied the Kinect to safe human–robot interaction (sHRI) has been discussed in a number of papers.[30–35] For example, Flacco et al. proposed a real-time collision avoidance approach[36] in which Kinect is used to evaluate the distances between moving obstacles, including people, and the robot. These distances are used to generate an execution motion trajectory for the robot. In addition, Rybski et al. presented a method that fuses data using Kinect and integrates that data into the robot's system.[37] A safety zone is generated around both the robot and the human, and a collision between the two is therefore avoided.

In this study, we used Kinect to obtain the relative velocity and distance between a person and a robot to calculate the hazard index. Additionally, integrated concepts of danger index (DI)[7] and RFDI will be applied to active–passive variable stiffness elastic actuator (APVSEA). For the purpose to ensure that the output performance of the system is consistent with the reference model, the model-matching control (MMC)[38,39] is employed.

This paper is organized as follows. Section 2 introduces the virtual fuse model and constructs it using a bond graph. It is necessary to understand the principle of the APVSEA as a bond graph in order to model the APVSEA, the RFDI system, and the virtual fuse. Therefore, the mechanism involved in the working principle of the APVSEA is presented and modelled using a bond graph in Section 3. Section 4 presents the concept of RFDI contraction, which is not only modeled on the APVSEA but also integrated the virtual fuse into the RFDI system. Section 5 presents the design of the rule of the virtual fuse switch and DI. Section 5.2 presents the verification of our approach with an experiment. Finally, the conclusion of the paper is discussed in Section 6.

2. Fuse Model Using a Bond Graph

As mentioned previously, when there are errors or unexpected situations in the system, additional measures are needed to ensure that the system is safe and reliable. A virtual fuse is thus set in the system. The fuse can be seen as a specific type of electrical switch. A fuse blows out in the same way that a switch is turned off if the unexpected stop condition is satisfied. Before modeling the virtual fuse, it is necessary to acquire an in-depth understanding of its basic principles. First, a fuse is either on or off, and these two conditions cannot co-exist. In other words, the function to cut off power is

https://doi.org/10.1017/S0263574720000715 Published online by Cambridge University Press

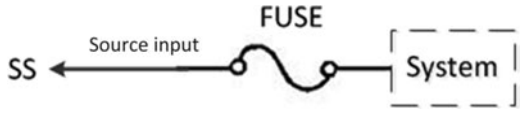

Fig. 1. Schematic diagram of a fuse.

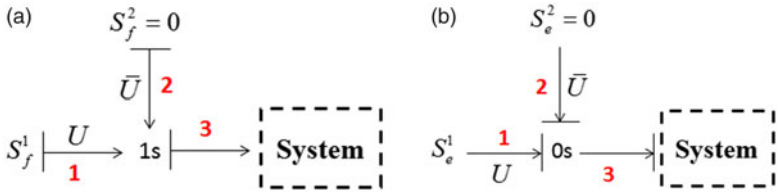

Fig. 2. Bond graph diagram of a fuse. (a) Flow source input and (b) effort source input.

regarded as another kind of energy source in addition to the real energy source; thus, there are two distinct energy sources connected to the fuse that are mutually exclusive.

If we consider a system such as that shown in Fig. 1, the flow and effort input are denoted as Sf and Se, respectively, and the fuse is located between the system and the source input.

Figure 2 shows a bond graph diagram of the system integrated with a fuse; bond numbers are shown in red, and 1s and 0s are the flow multijunction and effort multijunction, respectively. Two types of diagrams are used. The diagram on the left (a) presents the flow source input, and the effort source input is shown in the diagram on the right (b). As shown in Fig. 2, two types of energy sources are input into both of these bond graph diagrams. The working mechanism on both sides can be explained using the following formula:

(a) Left side of bond graph in Fig. 2
Junction flow source is equal to

$$Uf_1 + \bar{U}f_2, \tag{1}$$

$$e_1 = Ue_3, \tag{2}$$

$$e_2 = \bar{U}e_3. \tag{3}$$

(b) Right side of bond graph in Fig. 2
Junction effort source equals to

$$Ue_1 + \bar{U}e_2, \tag{4}$$

$$f_1 = Uf_3, \tag{5}$$

$$f_2 = \bar{U}f_3, \tag{6}$$

where U and $\bar{U}$ belong to 0 or 1 and are mutually exclusive; the values of U and $\bar{U}$ are different at the same time, which means that only one flow source can be input into the system. The effort source is represented as follows, where f_i represents the flow of the ith bond and the ith bond effort is denoted as e_i.

Note that the sources of S_f^2 and S_e^2 are 0 on each side of Fig. 2. This means that no energy source is being input into the system, which occurs when a fuse is broken. Therefore, it is possible to select the input into the system using U and $\bar{U}$, and the working mechanism is therefore similar to that of a switch.

3. The APVSEA Principle and Modelling

3.1. The APVSEA operation principle[40]

In order to achieve intrinsic safety, the APVSEA which has intrinsic safety properties is developed to address sHRI. As shown in Fig. 3, it consists of two parts: a serial elastic actuator and a mechanism that can actively or passively change the system stiffness. It is assembled using four components: DC

https://doi.org/10.1017/S0263574720000715 Published online by Cambridge University Press

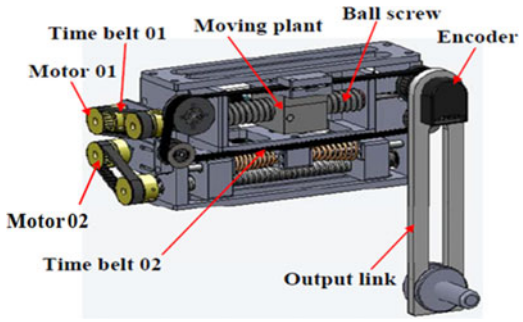

Fig. 3. APVSEA 3D diagram.

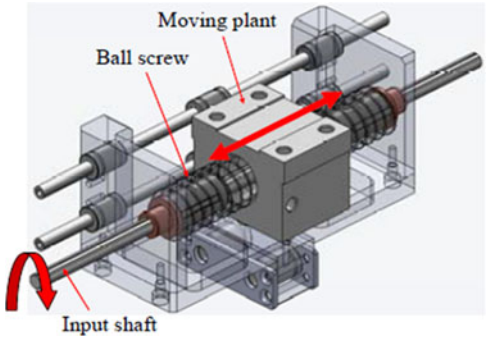

Fig. 4. Motor 01 rotates the ball screw, which moves the moving plant.

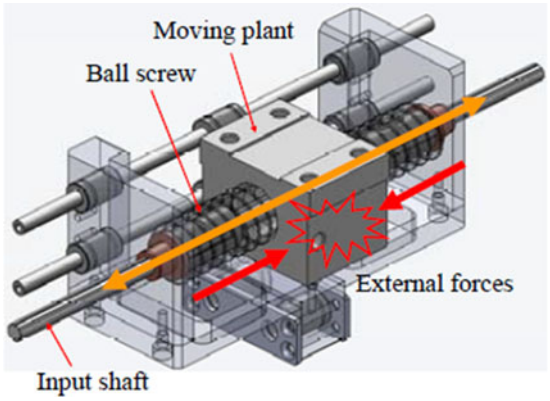

Fig. 5. External force generates axial slipping motion.

motors, a ball screw, a moving plant, and springs. The displacement of the spring is measured by the potentiometer which is behind the spring; three encoders are used to measure the angles of the motor and the output link.

As shown in Figs. 3 and 4, motor 01 rotates the output link of the APVSEA: motor 01 drives the ball screw though timing belt 01, the ball screw shifts the plant horizontally, and finally, timing belt 02 rotates the output link. In addition, motor 02 is used to change the stiffness of the APVSEA. As this work is focused on the FDI using the bond graph, the operational principle of motor 02 is only briefly discussed here, but it is described in detail in Wang and Huang.[40]

As an intrinsically safe mechanism, the APVSEA can absorb external forces. When these forces are applied to the output link, the moving plant is driven by them via timing belt 02, but the ball screw is not directly driven back by the moving plant. Instead, if there is an axial force generated by external forces, the moving plant will slip on the input shaft, and therefore, when the translation of the moving plant occurs, the springs of the APVSEA can absorb external forces using the connector, as shown in Fig. 5.

https://doi.org/10.1017/S0263574720000715 Published online by Cambridge University Press

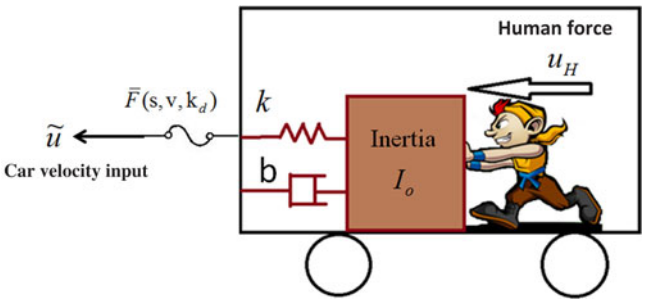

Fig. 6. APVSEA system simplistically represented as human pushing a mass–damper–spring system within a car.

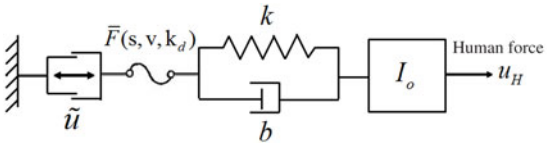

Fig. 7. Simplified APVSEA model.

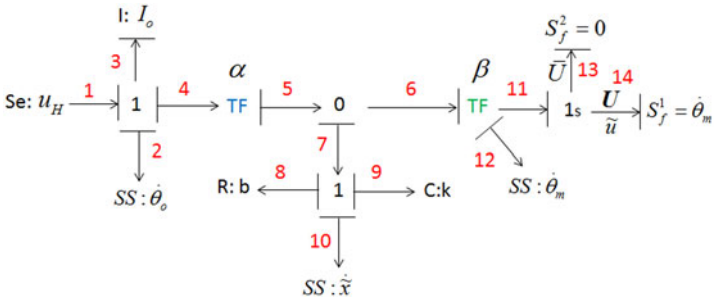

Fig. 8. APVSEA bond graph model.

3.2. Model of the APVSEA using a bond graph

In order to simplify the modeling of the APVSEA system, we can treat the model as a person pushing a spring–mass–damper system in a car with no ground contact friction, as shown in Fig. 6. The human force is inside the car and is unable to move the car forward. Therefore, the absolute position of the person can only be changed by the car moving, but the person cannot drive the car forward. In addition, we also add a fuse $\bar{F}$ (s, v, k_d) between the car velocity input and the vehicle.

Figure 7 shows a simplified APVSEA model that integrates a fuse, where $\tilde{u}$ is the control input from motor 01 and u_H is the external force applied by the user. The inertia, spring stiffness, and damping ratio are denoted by Io, k, and b, respectively. The function of the fuse is denoted by $\bar{F}$ (s, v, k_d), where s means the distance between a person and the system, the velocity of a person is represented by v, and kd is the desired stiffness command for the MMC. The detail about how the bond graph-based MMC adjusts the stiffness of the APVSEA was described in Cheng and Huang[38] and Cheng et al.[39]

Based on the APVSEA model, the system model is converted into a bond graph, as shown in Fig. 8, where the source–sensor element is represented as sensor source, effect source input (Se), and flow source input (Sf). They are defined as the sensor, the effort sources, and the flow sources, respectively. The bond graph elements of I, C, and R represent the inertia, spring, and damper in a mechanical domain, respectively. In addition, the bond graph junction elements are denoted as the black numbers 1 and 0, and the bond numbers are shown as the red numbers. There are two transformer elements; α and β represent the output link's rotational velocity, $\dot{\theta}_o$, and the motor rotational velocity, $\dot{\theta}_m$, respectively. Simultaneously, they are converting into a horizontal movement. Furthermore, u_H represents the human applied force to the output link, and the velocity of the spring is denoted as $\tilde{x}$.

https://doi.org/10.1017/S0263574720000715 Published online by Cambridge University Press

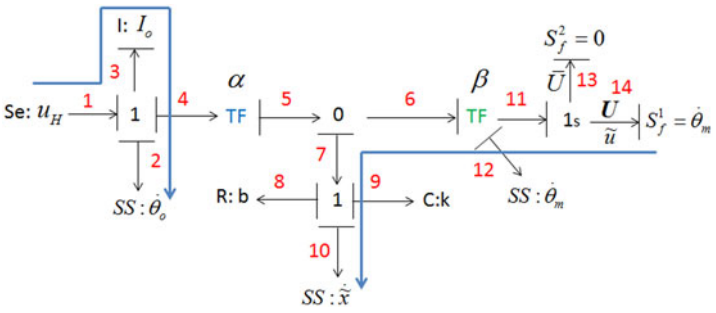

Fig. 9. Extended APVSEA bond graph.

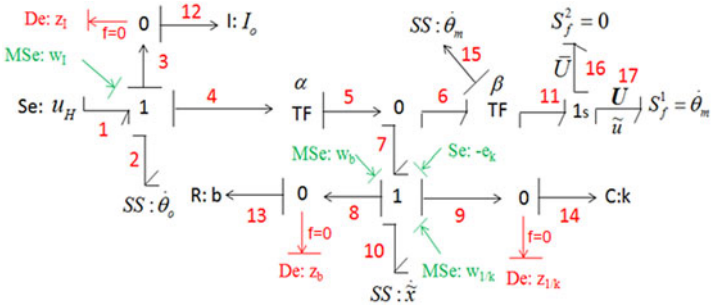

Fig. 10. Extended APVSEA bond graph including uncertain parts.

4. Robust FDI

4.1. Inverse model with uncertain part

In contrast to the traditional FDI, the RFDI can select a suitable isolation strategy based on the fault component if failures occur. The concept of RFDI will be applied to our study. The first step in the process of RFDI is to obtain the inverse APVSEA system from the bond graph model, as shown in Fig. 8. Meanwhile, a definition of the power lines is required, and this is represented as blue lines in Fig. 9. The process of transferring the original model to the inverse model involves changing each storage bond graph element passed through by a blue line into a bi-causal notation.

To derive an inverse system, we first define the uncertain elements of the APVSEA that are caused by unknown parameters or external noises. These unknown parameters behind each bond graph element require further definition, and the inverse system of the APVSEA, which is associated with uncertain parts, is given in Fig. 10.

The red and green bonds represent uncertainties that were previously defined by Djeziri *et al.*[26] These equations are listed as

$$w_b = -\frac{\Delta r}{r} z_b, \tag{7}$$

$$w_{1/k} = \frac{\Delta k}{k + \Delta k} z_{1/k}, \tag{8}$$

$$w_I = -\frac{\Delta I_o}{I} z_I, \tag{9}$$

where $z_b = b\dot{x}$, $z_{1/k} = kx$, and $z_I = I_o\ddot{\theta}_o$; Δr, Δk, and ΔI_o are uncertain parameters.

4.2. ARR equations and fault signature matrix

Subsequently, based on the bond graph, the ARR equations are generated to detect faults in the system. The following two equations can be obtained using the inverse bond graph shown in Fig. 10 as

$$\text{ARR1}: r_1 = u_H - I_o\ddot{\theta}_o - \alpha b\dot{x} - \alpha kx + N_1, \tag{10}$$

https://doi.org/10.1017/S0263574720000715 Published online by Cambridge University Press

Table I. The FSM of the APVSEA.

Component name	**A1**	**A2**	**A3**	M_b	I_b
External unexpected force	1	0	0	1	1
Output link encoder	1	1	1	1	1
Potentiometer	1	1	0	1	1
Cable/timing belt	0	1	0	1	0
Motor 01 encoder	0	1	1	1	1
Human motion fault	0	1	0	1	0

$$\begin{aligned}\text{ARR2}: r_2 = b\left[\beta\left(US_f^1 + \bar{U}S_f^2\right) - \alpha\dot{\theta}_o + \dot{x}\right] \\ + k\left(\beta\theta_m - \theta_o + x\right) + N_2,\end{aligned} \tag{11}$$

where $N1$ and $N2$ are the uncertain parts. It is very difficult to accurately measure the torque, u_H, that is applied to the output link. However, as the APVSEA is a serial elastic actuator, u_H can be measured using a potentiometer. The corresponding equations are

$$N_1 = \alpha\left(w_b + w_{1/k} - e_k\right) + w_I, \tag{12}$$

$$N_2 = w_b + w_{1/k} - e_k, \tag{13}$$

$$u_H = \alpha k x. \tag{14}$$

An initial condition, e_k, exists in Eq. (13); in this case, it is set at zero. However, the two ARR equations above are not able to completely detect each of the components concerned because they cannot be isolated using Eqs. (10) and (11). Therefore, it is necessary to add a new ARR equation to the APVSEA.

The output link is driven by a motor through the timing belt and ball screw. Therefore, there is a constant transmission ratio between the motor and the output link, which can be used to obtain the third ARR equation as

$$\text{ARR3}: r_3 = |\theta_m| - \gamma\,|\theta_o|\,, \tag{15}$$

where γ is the transmission ratio between the actuator rotation angle, θ_m, and the output link rotation angle, θ_o. Although there are no uncertain parameters existing in ARR3, an error can be generated due to elastic vibration. Therefore, it is still necessary to set a suitable threshold as

$$\begin{cases} |r_3| < s, & \text{no fault} \\ |r_3| \geq s, & \text{fault} \end{cases}, \tag{16}$$

where s is the ARR3 threshold value.

The fault signature matrix (FSM) is a fault index that can be used to isolate a faulty component. Each ARR equation has corresponding effect components, and identifying the effect components from each ARR equation is important when constructing the FSM. The FSM of the APVSEA is shown in Table I. If the residual equation is related to the component faults, the matrix index is 1; otherwise, it is 0. M_b denotes the monitoring ability of the component fault in the corresponding row. The index is set to 1 when a corresponding component is detected; otherwise, it is 0. This means that if the fault signature of the element is not zero, then $M_b = 1$. Similarly, I_b means that the component fault has an isolation ability. If no residual rows depend on each other, the I_b index is 1; otherwise, it is 0. In this way, the FSM is able to isolate faulty components.

Table I shows the results of five sensitive components using three residuals equations, where A_i represents the ith ARR equation that has been processed by the doubt index. Note that, if the elements in columns M_b and I_b are 1, it means the element can be measured and isolated. However, if the I_b value is 0 in the cable/timing belt and human motion fault columns, those faults cannot be isolated when the ARR index is $(A_1, A_2, A_3) = (0, 1, 0)$. In other words, if the fault alarm index is $(A_1, A_2, A_3) = (0, 1, 0)$, the system cannot determine which element (cable/timing belt or human motion fault column) is faulty. The RFDI method used in this article has been verified in our previous studies. This method is applied to zero gravity control in APVSEA, and it can effectively

https://doi.org/10.1017/S0263574720000715 Published online by Cambridge University Press

distinguish the failure of system parts and select appropriate control methods. The detailed context can be referred to in a previous publication.[27]

5. Fuse Switch Criterion

In this work, a virtual fuse is used to cut off the robot's power source. The main steps involved in switching the fuse are as follows:

Step 1: Kinect is a detector that measures the position of a human skeleton datum; it is used to acquire information pertaining to human motion (position and velocity).
Step 2: Calculating the distance between the human and the robot depends on the position data. We determine the shortest distance between a human joint and the robot. In this way, the relative velocity can also be determined.
Step 3: Human motion information is used to decide the required stiffness for the MMC that satisfies the Institut für Arbeitsschutz der Deutschen Gesetzlichen Unfallversicherung (IFA) criterion. IFA Berufsgenossenschaftlichen Institut für Arbeitsschutz (BGIA)[41] has been applied widely, and associated reports suggest the impact force tolerances of the human body.
Step 4: If the required stiffness can be realized by the robot, it is applied; if not, the fuse blows out.

5.1. Obtaining the information of a human using Kinect

The coordinates of a human body can be obtained using Kinect. However, most actual HRI cases involve injury to the head, shoulder, arm, and upper human body. Hence, as this work focuses on the upper human body, the Kinect device is used only to detect the head, shoulder, elbow, wrist, hand, and torso of a person.

The distance between a human arm and Kinect is denoted as

$$d_i^H(x_i^H, y_i^H, z_i^H), \tag{17}$$

where d_i^H represents the absolute distance between Kinect and a person, and the space coordinates of a human joint point are denoted as x_i^H, y_i^H, and z_i^H. We set the coordinate of Kinect to an original point (0,0,0). The absolute distance between Kinect and a robot is known in advance, and thus, the absolute position of the output link of the robot can be measured by the encoder which is located at the output link. The coordinates of the robot are denoted as

$$d_i^R(x_i^R, y_i^R, z_i^R), \tag{18}$$

where d_i^R represents the absolute distance between Kinect and the output link of the robot, and the space coordinates of the output link of the robot are denoted as x_i^R, y_i^R, and z_i^R.

We set the Kinect to the original point of world coordinates. It is easy to derive the equation for the output link in space, as follows:

$$L: \begin{cases} x_L = x_{OA} + \ell \sin\theta \cdot t \\ y_L = y_{OA} + \ell \cos\theta \cdot t \\ z_L = z_{OA} \end{cases}, \tag{19}$$

where x_{OA}, y_{OA}, and z_{OA} represent the original point of the APVSEA of each axis. The length of the output link is denoted by ℓ, θ is the rotation angle of the output link, and the dynamic parameter is represented by t.

In order to find the shortest distance between the output link and a human joint, it is necessary to set the shortest point, Q, in the output link. The point Q is defined as

$$Q\left(x_Q, y_Q, z_Q\right). \tag{20}$$

Then, the vector from each human joint, d^H, to the shortest Q is

$$\overline{d_i^H Q_i} = \left(x_i^Q - x_i^H \; y_i^Q - y_i^H \; z_i^Q - z_i^H\right). \tag{21}$$

If two lines in space are perpendicular to each other, then the inner product will equal zero. By making the inner product between vector L and vector $\overline{d_i^H Q_i}$ equal zero, the dynamic parameter *ti* can be found by the following equation:

https://doi.org/10.1017/S0263574720000715 Published online by Cambridge University Press

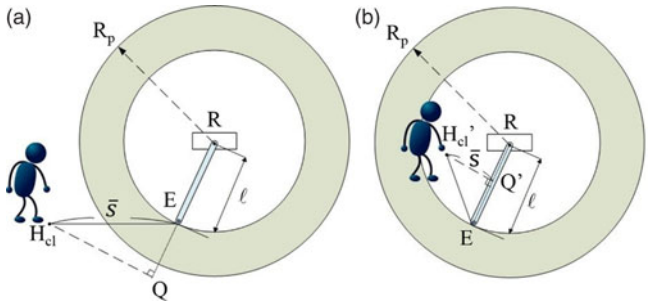

Fig. 11. The Q point in two situations: (a) out of working space and (b) within working space.

$$t_i = \frac{\left(x_i^H - x_{OA}\right)\sin\theta + \left(y_i^H - y_{OA}\right)\cos\theta}{\ell}. \tag{22}$$

After finding the dynamic parameter, ti, we can determine the shortest point, Q, between the robot and each human joint. However, Q may exist out of the rotation range of the output link, and therefore, two situations need to be considered:

a. When the Q point is located out of the output link working space, as presented in Figure 11(a), the $\bar{s}$ parameter will be the distance from the position of the person to the end point, E, of the output link.
b. When the Q' point exists in the output link working space, as shown in Fig. 11(b), the shortest distance, $\bar{s}$, is the length from the position of the person to the Q' point.

Therefore, by using the Euclidean distance, it is possible to calculate the shortest distance, $\bar{s}$, from each human joint to the output link, whether using point E or point Q. Then, by extracting the minimum value from the set of each joint, the shortest distance, S, is acquired by

$$S = \min\{\bar{s}_i\}, \tag{23}$$

where S is the distance of the closest two points of the human joints and APVSEA's output link.

Further, the current velocity, V_c, of the nearest joint can be acquired by the derivative information of the nearest corresponding joint.

5.2. *Calculating the requirement of stiffness*

The DI is used to evaluate the degree of danger to humans in this work, and the required stiffness can be calculated depending on the DI, which can be determined as a product of the relative distance f_D and velocity f_v:

$$DI = f_D \cdot f_v, \tag{24}$$

where DI means the danger index value. The formula for the relative distance f_D is

$$f_D = \begin{cases} 1, & S \le D_{\min} \\ H_D\left(\dfrac{1}{S} - \dfrac{1}{D_{\max}}\right)^2, & D_{\min} < S \le D_{\max} \\ 0, & S > D_{\max} \end{cases} \tag{25}$$

$$H_D = \left(\frac{D_{\min} D_{\max}}{D_{\min} - D_{\max}}\right)^2, \tag{26}$$

where S is the Euclidean distance between the robot and the nearest point of a human joint. The maximum safe distance is represented as D_{max}; D_{min} is the minimum safe distance.

https://doi.org/10.1017/S0263574720000715 Published online by Cambridge University Press

The parameter of f_v can be defined as follows:

$$f_\upsilon = \begin{cases} 1, & V_C \geq V_{\max} \\ H_\upsilon(V_C - V_{\min}), & V_{\min} \leq V_C < V_{\max}, \\ 0, & V_C < V_{\min} \end{cases} \tag{27}$$

$$H_\upsilon = \left(\frac{1}{V_{\max} - V_{\min}}\right), \tag{28}$$

where V_c is the nearest joint current velocity, and V_{min} represents the minimum velocity. When V_c is smaller than V_{min}, the operator will not be harmed during an HRI even if a collision occurs. However, the operator may suffer injury when the relative velocity is more than V_{max}, even if the stiffness of the system is changed to minimum. Hence, the parameters of V_{min} and V_{max} must be modified based on the stiffness of the robot and the tolerance impact force of the human body.

In this work, we designed the V_{max} as

$$V_{\max} = \frac{F_{IMF}}{k_{\min} \times T_{rea}}, \tag{29}$$

where k_{min} defines the minimum stiffness that the robot can be modified to and F_{IMF} is the tolerance impact force for a human body. When a human suffers an impact, the human reaction time is defined as T_{rea}.

Once the DI value is calculated, it is utilized to generate the total required stiffness command, k_T, for the whole system using the following equation:

$$k_T = k_{\max} - DI\ (k_{\max} - k_{\min}), \tag{30}$$

where the total required stiffness is the stiffness of the whole system.

5.3. Determining the fuse switch criterion

After obtaining the required stiffness (k_T), as shown in Eq. (30), it is necessary to determine the required stiffness that implies a risk for sHRI. There are limit constraints in the mechanism and properties of every robot and machine; even when the system stiffness has been adjusted to the lowest level, it is still possible to cause harm to the operator. As previously discussed, the virtual fuse provides the second protection, and Eq. (31) is used to judge whether the fuse has been blown or not. The equation only operates when the DI value equals 1, which means that a collision may happen at any time:

$$\lambda = F_{IMF} - k_T \cdot \beta \cdot \frac{1}{2}\ddot{\theta}_m T^2. \tag{31}$$

In Eq. (31), $\ddot{\theta}_m$ is the angular acceleration of the motor, β represents the coefficient of converting the motor rotational velocity of $\dot{\theta}_m$ into a horizontal movement, and T is a constant value that was set to 0.1 s. The equation shows that a collision between a human and a robot occurs based on stiffness, k_T. When the reaction time of a human is 0.1 s, Eq. (31) will check whether the impact force from the robot is greater than F_{IMF}. Therefore, if λ is greater than 0, it is possible to determine that a person will not suffer injury from the robot, even if a collision occurs. In contrast, the fuse will blow out when the λ value is negative.

Therefore, the above discussion can be represented as

$$U = \begin{cases} 1, \lambda > 0 \\ 0, \lambda \leq 0 \end{cases}, \tag{32}$$

$$\bar{U} = \begin{cases} 0, \lambda > 0 \\ 1, \lambda \leq 0 \end{cases}. \tag{33}$$

6. Experiments

For this paper, an experiment was conducted to verify our approach. Suppose that an operator is close to the APVSEA robot and tries to pick up a bottle from the ground near the working area of the

https://doi.org/10.1017/S0263574720000715 Published online by Cambridge University Press

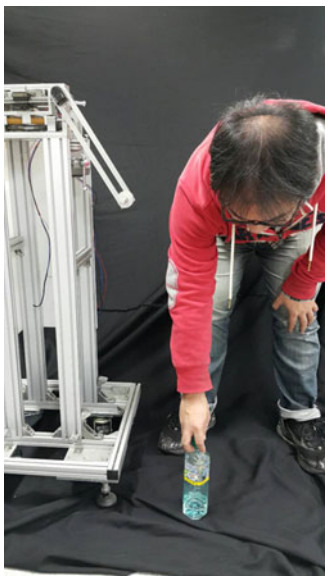

Fig. 12. Operator picks up the bottle from the ground.

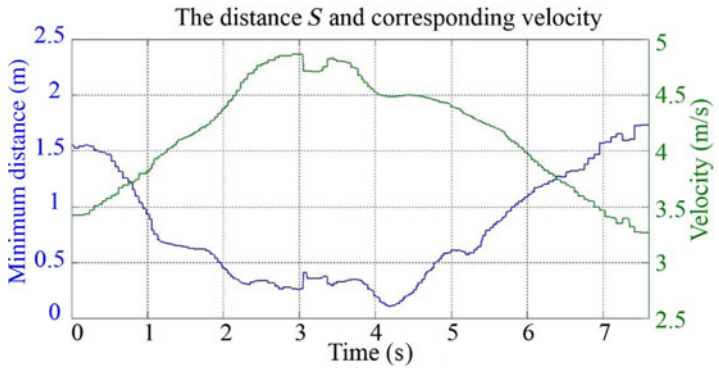

Fig. 13. Distance, S, and velocity between the human joint and the robot.

APVSEA, as shown in Fig. 12. In the end, the operator turns away from the APVSEA after picking up the bottle. The experimental scenario demonstrated that the operator picked up the bottle quickly.

In this scenario, the operator tried to pick up the bottle from the ground near the robot at a fast moving speed. Figure 13 shows the minimum distance, S, and velocity between the human joints and the APVSEA. The blue curve represents the minimum distance, S, between the operator and the APVSEA, and the corresponding velocity of the minimum distance is represented by the green curve. As shown in Fig. 13, the operator was very close to the APVSEA, from 2.3 to 4.6 s. The velocity reached a maximum when the operator bent down. It must be noted that the operator bent down very quickly (4.8 m/s), and this is the action that can generate injury when collisions occur.

After attaining the minimum distance and corresponding velocity, the required stiffness, k_T, can be calculated for the MMC, as shown in Fig. 14. The figure shows that when the required stiffness, k_T, equals the minimum value, the system judges whether the stiffness is adequate to protect a human from a collision by using Eq. (31). In this experiment, the system adopts Eq. (31) at 2.3 s. Figure 15 shows the results of calculating λ with Eq. (31). The red region is the detectable area, which means that the DI value is 1, and therefore, the required stiffness, k_T, is equal to the minimum value. As shown in the result, the value of λ is negative, and therefore, injury would occur even though the system's stiffness has been adjusted to the minimum.

As the red area indicates, human injury can occur, and thus, index U and $\bar{U}$ are also changed; results are presented in Fig. 16. The blue line demonstrates that the index value of U was changed to 0 from 2.3 to 4.6 s. In contrast, the index value of $\bar{U}$ (green dotted line) was modified to 1 in the same

https://doi.org/10.1017/S0263574720000715 Published online by Cambridge University Press

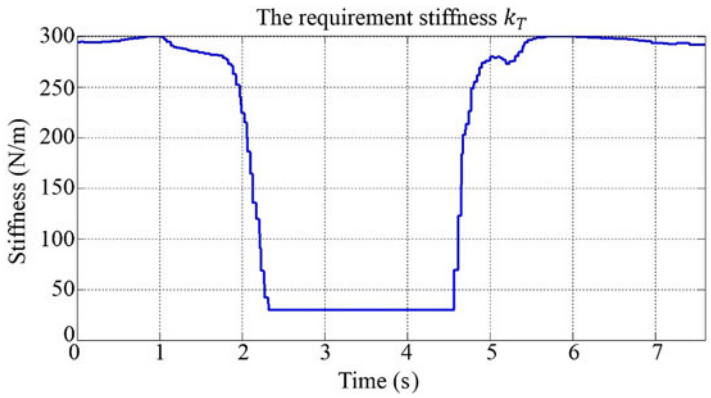

Fig. 14. Required stiffness diagram.

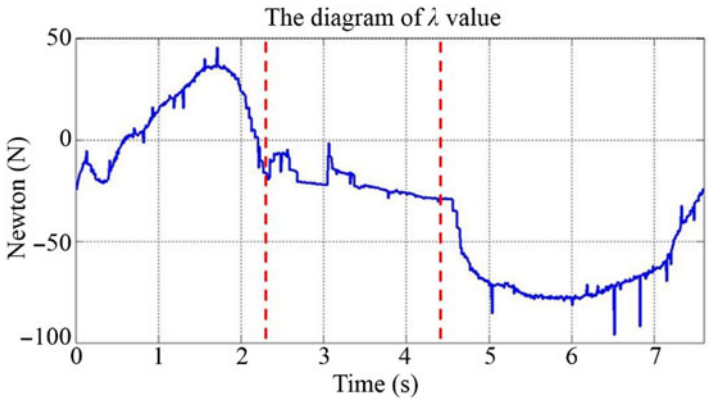

Fig. 15. The λ value is less than zero in the red region.

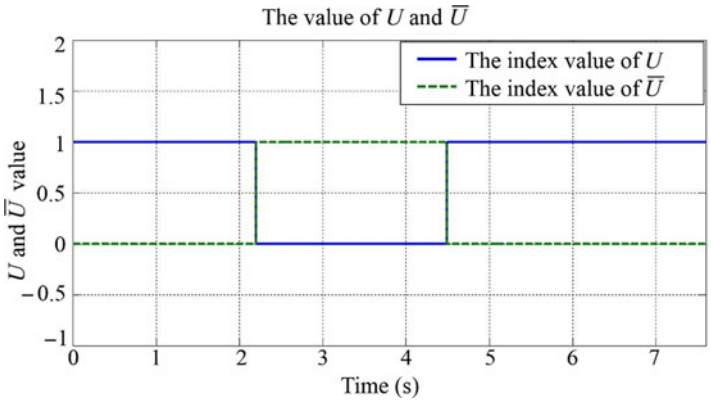

Fig. 16. U and $\bar{U}$ values changed at 2.3 s.

time span. When $\bar{U}$ is equal to 1, it implies the fuse has been blown. The ARR2 equation generates a fault sign (ARR2 = 1) when $\bar{U}$ = 1 because the equation is not balanced. However, the values of ARR1 and ARR3 are also 0, as shown in Fig. 17, and therefore, the fault can be isolated using the FSM, as shown in Table I.

The APVSEA was therefore stopped due to the human motion fault, and Fig. 18 represents the APVSEA's output link rotation phenomena. To protect the operator in this situation, once a collision occurs, the system judges if the APVSEA will injure the operator and stops the motion of the APVSEA input motor. Hence, the output link is stopped at 2.3 s, as shown in Fig. 18, which guarantees that the operator will not be subjected to any risk from the robot.

https://doi.org/10.1017/S0263574720000715 Published online by Cambridge University Press

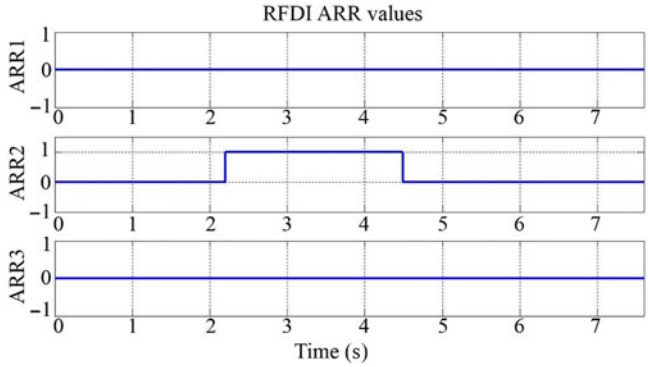

Fig. 17. RFDI ARR values can indicate which component is at fault.

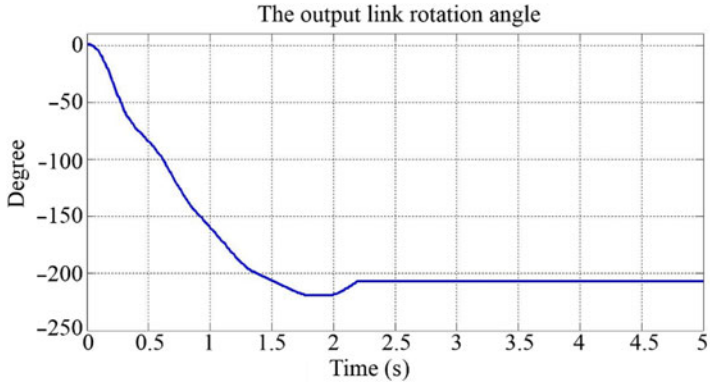

Fig. 18. Output link stopped at 2.3 s.

7. Conclusion

In this article, a concept combining DI and RFDI was presented to avoid APVSEA causing injury to users due to mechanical limit constraints. Furthermore, the bond graph method for APVSEA modeling and the MMC was also summarized.

The experimental results showed that the proposed concept could be used as a post-collision safety strategy. APVSEA can actively change joint stiffness with the change of DI, so as to ensure the effective reduction of the impact force during the collision. In addition, the proposed approach is able to detect whether the stiffness command is working to protect a person from injury, and the virtual fuse is blown for an emergency stop if the lowest stiffness command still generates any potential risk to a person. It is worth noting that the RFDI method proposed in this paper cannot only stop the robot immediately when safety problems occur but also effectively detect the failure of other components. This concept can effectively confirm the fault mode and provide additional protection measures to ensure the safety of users.

Supplementary material

To view supplementary material for this article, please visit https://doi.org/10.1017/S0263574720000715.

References

1. T. S. Tadele, T. de Vries and S. Stramigioli, "The safety of domestic robotics: A survey of various safety-related publications," *IEEE Robot. Autom. Mag.* **21**(3), 134–142 (2014).
2. A. Bicchi, M. A. Peshkin and J. E. Colgate, "Safety for Physical Human–Robot Interaction," **In**: *Springer Handbook of Robotics* (B. Siciliano and O. Khatib, eds.), Ch. 58 (Springer, Berlin, 2008) pp. 1335–1348.
3. A. Bicchi, M. Bavaro, G. Boccadamo, D. D. Carli, R. Filippini, G. Grioli, M. Piccigallo, A. Rosi, R. Schiavi, S. Sen and G. Tonietti, "Physical human-robot interaction: Dependability, safety, and performance," *Proceedings of the IEEE International Workshop on Advanced Motion Control (AMC)*, Trento, Italy (March 2008), pp. 9–14.

4. M. B. Huang and H. P. Huang, "Innovative human-like dual robotic hand mechatronic design and its chess-playing experiment," *IEEE Access.* **7**(1), 7872–7888 (2019).
5. P. A. Lasota, T. Fong and J. A. Shah, "A survey of methods for safe human–robot interaction," *Found. Trends Robot.* **5**(4), 261–349 (2017).
6. V. Villani, F. Pini, F. Leali and C. Secchi, "Survey on human–robot collaboration in industrial settings: Safety, intuitive interfaces and applications," *Mechatronics* **55**, 248–266 (2018).
7. H. Y. Ting, H. K. Hsu, M. B. Huang and H. P. Huang, "Safety of human-robot interaction: Concepts and implementation based on robot-related standards," *J. Chinese Soc. Mech. Engin. (JCSME)* **41**(2), 199–209 (2020).
8. Y. Yamada, T. Morizono, Y. Umetani and H. Takahashi, "Highly soft viscoelastic robot skin with a contact object-location-sensing capability," *IEEE Tran. Ind. Elec.* **52**(4), 960–968 (2005).
9. R. V. Ham, T. G. Sugar, B. Vanderborght, K. W. Hollander and D. Lefeber, "Compliant actuator designs," *IEEE Robot. Autom. Mag.* **16**(3), 81–94 (2009).
10. J. J. Park, Y. J. Lee, J. B. Song and H. S. Kim, "Safe Joint Mechanism Based on Nonlinear Stiffness for Safe Human-Robot Collision," *Proceedings of the IEEE International Conference on Robotics and Automation (ICRA),* Pasadena, California (2008), pp. 2177–2182.
11. R. Schiavi, G. Grioli, S. Sen and A. Bicchi, "VSA-II: A Novel Prototype of Variable Stiffness Actuator for Safe and Performing Robots Interacting with Humans," *Proceedings of the IEEE International Conference on Robotics and Automation (ICRA),* Pasadena, California (May 2008), pp. 2171–2176.
12. G. Tonietti, R. Schiavi and A. Bicchi, "Design and Control of a Variable Stiffness Actuator for Safe and Fast Physical Human/Robot Interaction," *Proceedings of the 2005 IEEE International Conference on Robotics and Automation (ICRA)*, Barcelona, Spain (April 2005), pp. 526–531.
13. N. D. Vuong, R. Li, C. M. Chew, A. Jafari and J. Polden, "A novel variable stiffness mechanism with linear spring characteristic for machining operations," *Robotica* **35**(7), 1627–1637 (2017).
14. S. Wolf, T. Bahls, M. Chalon, W. Friedl, M. Grebenstein, H. Höppner, M. Kühne, D. Lakatos, N. Mansfeld, M. C. Özparpucu, F. Petit, J. Reinecke, R. Weitschat and A. Albu-Schäffer, "Soft Robotics with Variable Stiffness Actuators: Tough Robots for Soft Human Robot Interaction," **In**: *Soft Robotics* (A. Verl, A. Albu-Schäffer, O. Brock and A. Raatz, eds.), Ch. 20 (Springer, Berlin, 2015) pp. 231–254.
15. X. Li, Xiang, Y. H. Liu and H. Yu, "Adaptive Impedance Control for Compliantly Actuated Robots with a Unified Safety Measure." *Proceedings of the World Congress on Intelligent Control and Automation (WCICA)*, Changsha, China (July 2018), pp. 444–449.
16. I. Hwang, S. Kim, Y. Kim and C. E. Seah, "A survey of fault detection, isolation, and reconfiguration methods," *IEEE Tran. Control Sys. Tech.* **18**(3), 636–653 (2010).
17. V. Venkatasubramanian, R. Rengaswamy, K. Yin and S. N. Kavuri, "A review of process fault detection and diagnosis part I: Quantitative model-based methods," *Comp. Chem. Eng.* **27**(3), 293–311 (2003).
18. V. Venkatasubramanian, R. Rengaswamy, K. Yin and S. N. Kavuri, "A review of process fault detection and diagnosis part II: Qualitative models and search strategies," *Comp. Chem. Eng.* **27**(3), 313–326 (2003).
19. V. Venkatasubramanian, R. Rengaswamy, K. Yin and S. N. Kavuri, "A review of process fault detection and diagnosis part III: Process history based methods," *Comp. Chem. Eng.* **27**(3), 327–346 (2003).
20. K. Medjaher, "A Bond Graph Model-based Fault Detection and Isolation," **In**: *Maintenance Modelling and Applications* (J. Andrews, CH. Bérenguer and L. Jackson, eds.), Ch. 6 (Det Norske Veritas, Hovik, 2011) pp. 497–506.
21. A. K. Samantaray and B. O. Belkacem, "Bond Graph Model-based Quantitative FDI," **In**: *Model-based Process Supervision: A Bond Graph Approach*, Ch. 5 (Springer, London, 2008), pp. 177–228.
22. W. Bouallegue, S. B. Bouabdallah and M. Tagina, "A New Adaptive Fuzzy FDI Method for Bond Graph Uncertain Parameters Systems," *Proceedings of the IEEE International Conference on Electronics, Circuits and Systems (ICECS),* Beirut, Lebanon (December, 2011), pp. 643–648.
23. W. Bouallegue, S. B. Bouabdallah and M. Tagina, "Causal Approaches and Fuzzy Logic in FDI of Bond Graph Uncertain Parameters Systems," *Proceedings of the International Conference on Communications, Computing and Control Applications (CCCA),* Hammamet, Tunisia (March 2011), pp. 1–6.
24. K. Emami, B. Nener, V. Sreeram, H. Trinh and T. Fernando, "A Fault Detection Technique for Dynamical Systems," *Proceedings of the IEEE Conference on Industrial and Information Systems (ICIIS),* Sri Lanka (August 2013), pp. 201–206.
25. B. Pourbabaee, N. Meskin and K. Khorasani, "Sensor Fault Detection and Isolation using Multiple Robust Filters for Linear Systems with Time-Varying Parameter Uncertainty and Error Variance Constraints," *Proceedings of the IEEE Conference on Control Applications (CCA),* Juan Les Antibes, France (October 2014), pp. 382–389.
26. M. A. Djeziri, R. Merzouki, B. O. Bunamama and G. Dauphin-Tanguy, "Robust Fault Diagnosis by Using Bond Graph Approach," *IEEE Trans. Mechatron.* **12**(6), 599–611 (2007).
27. P. J. Cheng and H. P. Huang, "Robust Fault Detection and Isolation using Bond Graph for an Active-Passive Variable Serial Elastic Actuator," *Int. J. Robot. Auto.* **6**(2), 29–47 (2015).
28. H. Liu and L. Yu, "Analytical Method of Fault Detection and Isolation Based on Bond Graph for Electromechanical Actuator," *Proceedings of the 2017 IEEE International Conference on Mechatronics and Automation (ICMA),* Takamatsu, Japan (August 2017), pp. 393–397.
29. A. Mojallal and S. Lotfifard, "Multi-physics graphical model based fault detection and isolation in wind turbines," *IEEE Trans. Smart Grid* **9**(6), 5599–5612 (2018).

https://doi.org/10.1017/S0263574720000715 Published online by Cambridge University Press

30. D. Sidobre, X. Broquère, J. Mainprice, E. Burattini, A. Finzi, S. Rossi and M. Staffa, "Human–Robot interaction," **In**: *Advanced Bimanual Manipulation* (B. Siciliano, ed.), Ch. 3 (Springer, Berlin, 2012) pp. 123–172.
31. T. Beyl, P. Nicolai, J. Raczkowsky, H. Worn, M. D. Comparetti and E. D. Momi, "Multi Kinect People Detection for Intuitive and Safe Human Robot Cooperation in The Operating Room," *Proceedings of the International Conference on Advanced Robotics (ICAR),* Montevideo, Uruguay (November 2013), pp. 1–6.
32. A. D. Luca and F. Flacco, "Integrated Control for pHRI: Collision Avoidance, Detection, Reaction and Collaboration," *Proceedings of the IEEE RAS & EMBS International Conference on Biomedical Robotics and Biomechatronics (BioRob),* Rome, Italy (June 2012), pp. 288–295.
33. C. Morato, K. N. Kaipa, B. Zhao and S. K. Gupta, "Toward safe human robot collaboration by using multiple kinects based real-time human tracking," *J. Com. Info. Sci. Engin.* **14**(1), 0110061–0110069 (2014).
34. G. Randelli, T. Bonanni, L. Iocchi and D. Nardi, "Knowledge acquisition through human–robot multimodal interaction," *Intel. Serv. Robot.* **6**(1), 19–31 (2013).
35. S. S. Yun, "A gaze control of socially interactive robots in multiple-person interaction," *Robotica* **35**(11), 2122–2138 (2017).
36. F. Flacco, T. Kroger, A. D. Luca and O. Khatib, "A Depth Space Approach to Human-Robot Collision Avoidance," *Proceedings of the IEEE International Conference on Robotics and Automation (ICRA),* Saint Paul, Minnesota (May 2012), pp. 338–345.
37. P. Rybski, P. Anderson-Sprecher, D. Huber, C. Niessl and R. Simmons, "Sensor Fusion for Human Safety in Industrial Workcells," *Proceedings of the IEEE/RSJ International Conference on Intelligent Robots and Systems (IROS),* Vilamoura, Portugal (October 2012), pp. 3612–3619.
38. P. J. Cheng and H. P. Huang, "Model matching contorl for an active-passive variable stiffness actuator," *Int. J. Robot. Auto.* **6**(3), 48–64 (2015).
39. P. J. Cheng, H. Y. Ting and H. P. Huang, "Safe human robot inter action using model matching control," *J. Chinese Soc. Mech. Engin. (JCSME)* **37**(6), 587–596 (2016).
40. R. J. Wang and H. P. Huang, "Mechanically stiffness-adjustable actuator using a leaf spring for safe physical human-robot interaction," *Mechanika* **18**(1), 77–83 (2012).
41. IFA, BG/BGIA risk assessment recommendations according to machinery directive: Design of workplaces with collaborative robots (2013).

https://doi.org/10.1017/S0263574720000715 Published online by Cambridge University Press